Accurate real-time modeling for multiple-blow forging

David Uribe[1] · Camille Durand[1] · Cyrille Baudouin[1] · Régis Bigot[1]

Abstract
Numerical simulations are crucial for predicting outcomes in forging processes but often neglect dynamic interactions within forming tools and presses. This study proposes an approach for achieving accurate real-time prediction of forging outcomes. Initially, a simulation-based surrogate model is developed to replicate key process characteristics related to the billet, enabling prediction of geometry, deformation field, and forging load after an upsetting operation. Subsequently, this model is integrated with a mass-spring-damper model representing the behavior of forging machine and tools. This integration enables the prediction of blow efficiency and energy distribution after each blow, including plastic, elastic, damping, and frictional energy of the upsetting operation. The approach is validated by comparing predictions with experimental results. The coupled model outperformed Finite Element Method (FEM) predictions, exhibiting mean absolute errors (MAE) below 0.1 mm and mean absolute percentage errors (MAPE) below 1% in geometry predictions. Deformation field predictions showed errors below 0.05 mm/mm, and load-displacement curves closely matched experimental data. Blow efficiency predictions aligned well with experimental results, demonstrating a mean absolute error below 1.1%. The observed energy distribution correlated with literature findings, underscoring the model's fidelity. The proposed methodology presents a promising approach for accurate real-time prediction of forging outcomes.

Keywords Forging · Numerical simulation · Real-time · Surrogate model · Mass-spring-damper model · Digital twin

Introduction

In the realm of forging processes, the paramount role of numerical simulations is acknowledged, providing predictive insights without the necessity for exhaustive physical experimentation [1]. These simulations excel in estimating variables such as deformation fields, stress distributions, and temperature profiles, often challenging or even impossible to measure directly. However, while numerical simulations tailored for forging processes adeptly forecast outcomes and explore various billet-related scenarios, the intricate dynamics inherent in forming tools and presses are frequently overlooked.

This oversight becomes apparent in the simplified modeling approaches commonly employed for presses and tools, where tools are often depicted as purely elastic elements characterized by parameters like Young's modulus and Poisson's ratio, and presses are typically simplified using an equivalent stiffness value, also known as a 1D formulation of the machine [2, 3]. Such simplistic representations fail to capture the nuanced energy interactions inherent in forging processes, particularly when dealing with energy-driven machines like screw presses and power hammers [4]. Consequently, if these complex dynamic interactions between the press, workpiece, and tooling, are not adequately accounted for, the predictions of finite element models may prove insufficient [5]. This inadequacy arises from the incomplete consideration of factors such as blow efficiency or energy losses. The blow's efficiency is primarily determined by the work-hardened state of the billet itself and its shape as it undergoes plastic deformation [6], and its interaction with the press and tooling. Therefore, considering these

David Uribe
david_santiago.uribe_espitia@ensam.eu

Camille Durand
camille.durand@ensam.eu

Cyrille Baudouin
cyrille.baudouin@ensam.eu

Régis Bigot
regis.bigot@ensam.eu

[1] Arts et Métiers Institute of Technology, Université de Lorraine, LCFC, Metz F-57070, France

phenomena is crucial for accurately predicting the forging outcomes. The literature has explored various approaches to represent the dynamics of forging machines, spanning from the finite element modelling of the machines [7, 8] to methods like multi-body systems [9, 10], explicit dynamic methods [11, 12], and the mass-spring-damper systems [13, 14]. In particular, mass-spring-damper systems are noted for their suitability in real-time applications, as they offer reasonably accurate results with significantly lower computation times compared to other methods [15]. While integrating these models with numerical simulations of the forging process can yield better results, they do not reduce the inherent computational demands of these simulations, which remains a significant limitation for real-time control applications in forging.

To address this real-time challenge, surrogate models have emerged as promising alternatives in various manufacturing scenarios. They offer a simplified representation of the original system, capable of reproducing its key features with reduced computational cost and higher speed [16]. While simulations excel in providing precise predictions of system behaviors, surrogate models provide the advantage of delivering faster and more cost-effective predictions with acceptable accuracy.

Despite the relatively limited adoption in the forming domain until recently, surrogate models have gained extensive traction and proven successful in various manufacturing processes [17–20]. In sheet metal forming, surrogate models have found applications in predicting critical parameters such as rolling load [21], Forming Limit Diagrams (FLDs) [22], springback effects [23, 24], and deep drawing parameters [25]. Similarly, in forging operations, surrogate models have been employed to predict the shaping of billets and deformation fields in upsetting operations [26], tool design [27], as well as to forecast grain size evolution [28].

But with surrogate models, dealing with multi-dimensional data, such as fields, curves, or complex geometries, often poses challenges because surrogate models generally perform better with scalar data. To address this issue, model reduction techniques are employed to simplify the data, which is crucial for improving both the efficiency and the accuracy of predictions. This simplification is typically achieved through reduced order modeling, which reduce the dimensionality of complex datasets while preserving the essential dynamics of the system. In the context of metal forming, various techniques such as Proper Generalized Decomposition (PGD), Proper Orthogonal Decomposition (POD), Reduced Basis (RB) method, and Hyper-reduction are commonly used to achieve this reduction [29, 30]. POD-based surrogate models were chosen in this paper for their wide applicability in metal forming processes, encompassing applications such as displacement vectors [22], spring-back compensation [24], temperature fields [31], deformation fields [32], stress fields [33], and other representations.

In this study, a three-step approach is proposed to achieve accurate real-time prediction of forging outcomes. Firstly, a POD-based surrogate model is developed capable of replicating key billet-related process characteristics with enhanced computational efficiency [16]. Subsequently, this model is coupled with a mass-spring-damper model of the forging machine and tools to comprehensively capture dynamic interactions. Finally, the approach is validated by comparing predictions with experimental results, thereby verifying the effectiveness of the model in predicting key forging process parameters.

Materials

Experimental setup

The study focuses the upsetting process of a cylindrical pure copper billet subjected to multiple blows using a screw press. In this process, a billet characterized by its Initial Diameter (D_0) and Initial Height (H_0) is repeatedly forged at room temperature along its revolution axis. The initial geometries of the billets are within the following variation ranges:

- $D_0 = [15 - 35]\ mm$
- $SR = H_0/D_0 = [1.5 - 2]$

Here, SR represents the slenderness ratio. Throughout the successive blows, both the metallurgical properties and the geometry of the billet undergo changes. Following the initial blow, the billet's geometry deviates from its cylindrical shape due to friction conditions, resulting in a bulging profile (BP). Achieving precise control over the final geometry of the upset workpiece necessitates understanding the forging energy setup for each blow (E_i), considering the workpiece's initial, intermediate, and final states (see Fig. 1).

The billet is forged using the *LASCO SPR400* screw press on the VULCAIN platform at Arts et Métiers Metz in France, which is part of the Laboratory of Design, Manufacturing, and Control (see Fig. 2). This press can provide a maximum forging energy of 28,9 kJ for a ram speed of 680 mm/s. The press is controlled by a setup energy adjustable from 1 to 100% of its maximum capacity. Tools with smoothed flat dies and a graphite-based aerosol lubricant were used for the upsetting operations.

During the forging operations, the displacement of the ram is measured using three laser sensors *MicroEpsilon®optoNCDT ILD 1401 – 200* positioned at

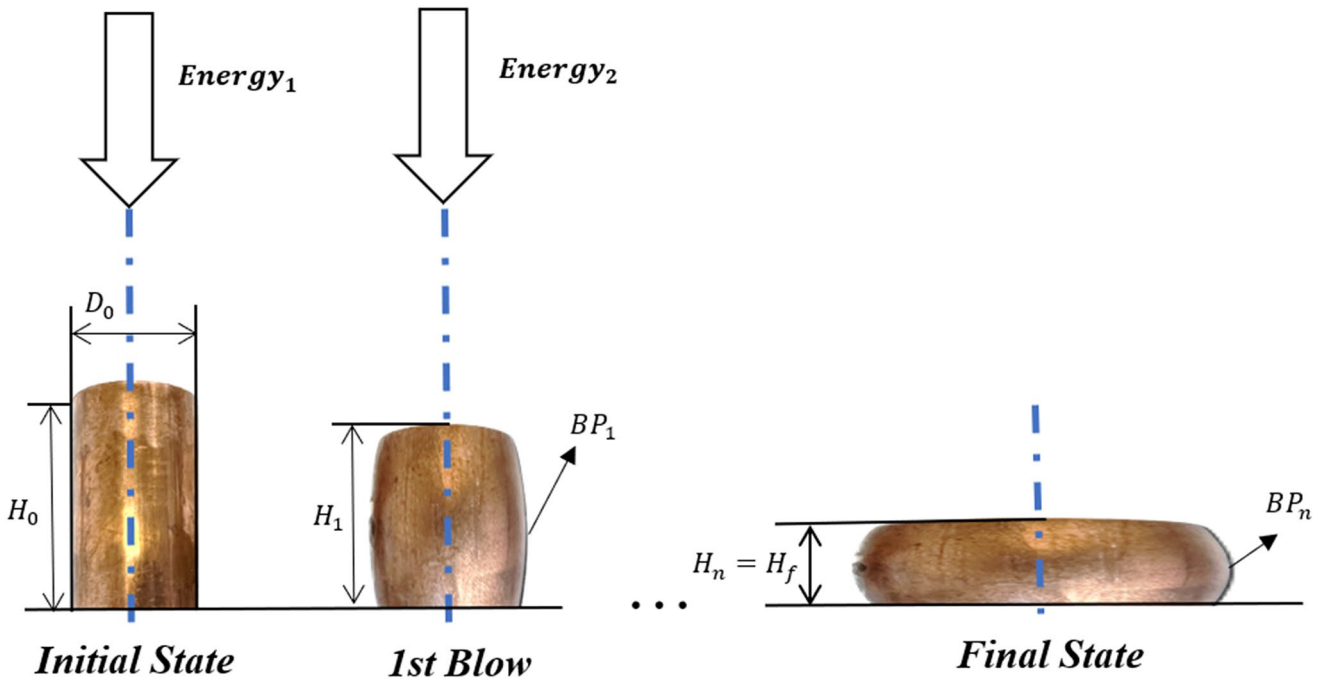

Fig. 1 Multiple-blow upsetting schematic

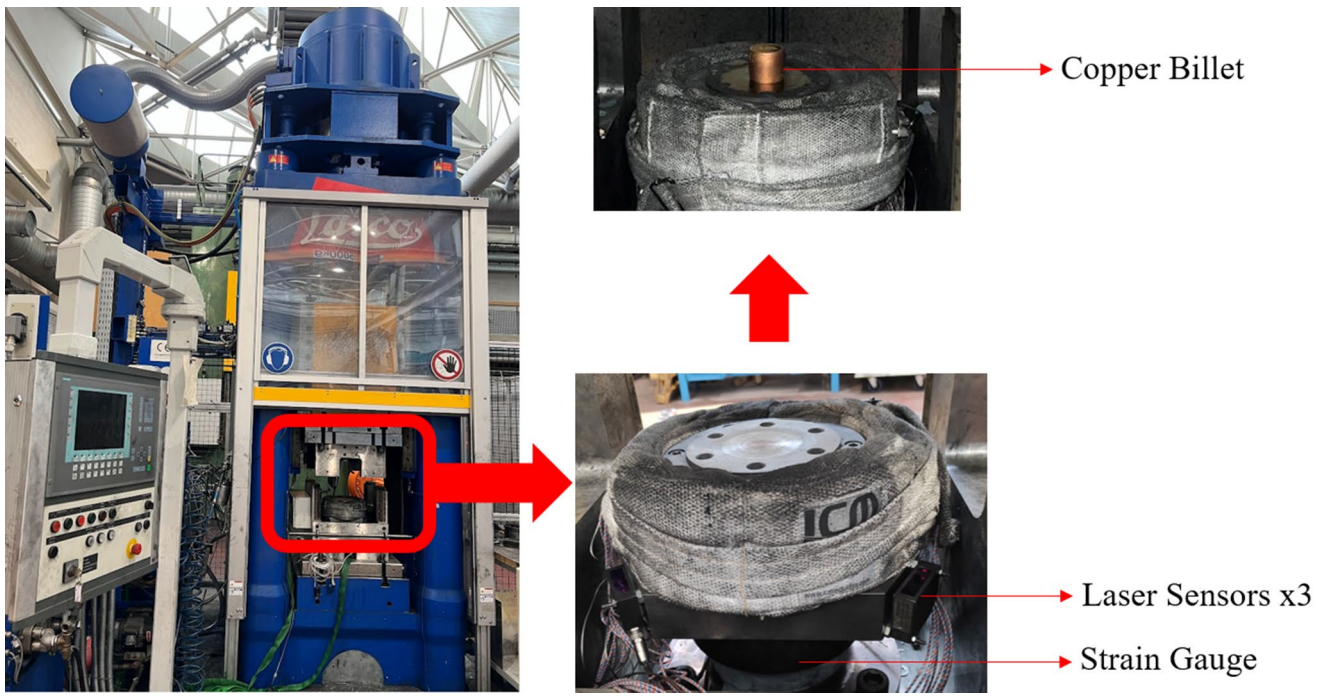

Fig. 2 Experimental setup featuring the screw press, tooling, sensors, and billet

120-degree intervals in the plane of the lower tool. Additionally, the axial forging load is measured using a deformation gauge *Doerler 29,744 – C04121* installed in a plate within the lower tool.

The experimental geometries of the billets after each blow were obtained using a high-resolution 3D optical scanner, the *GOM ATOS II Triple Scan*® (see Fig. 3a). Each billet's geometry resulted in a 3D file (.stl), which was then processed using GOM Inspect® Software to extract the corresponding bulging profile for analysis as a set of 2D scattered points. Specifically, a mean profile was extracted by defining a central axis for the entire volume and making 18

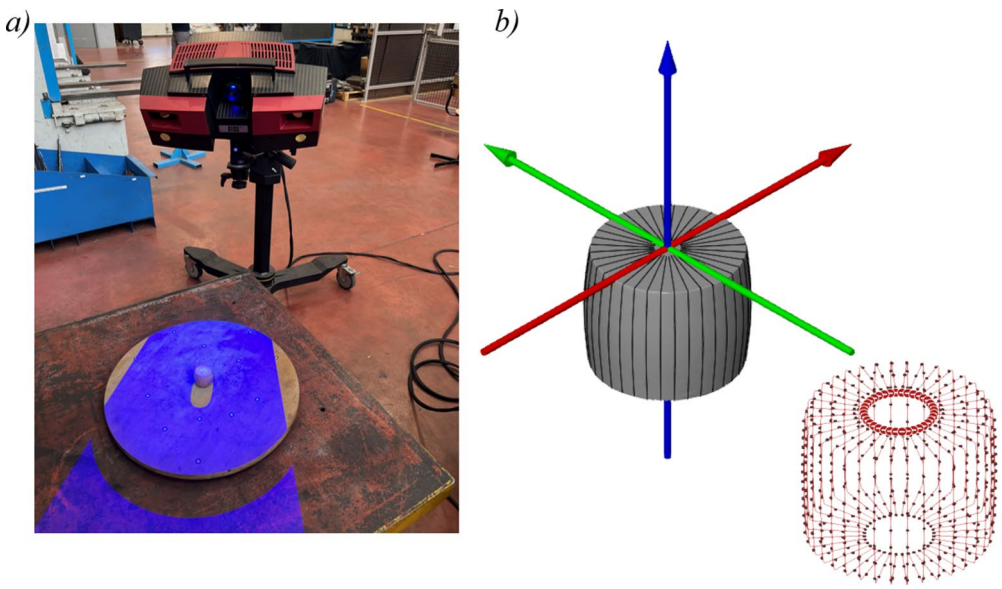

Fig. 3 Geometry extraction: **a**) Optical 3D Scanner. **b**) Post-analysis

sections, resulting in 36 axial symmetric cuts, as depicted in Fig. 3b.

Numerical Model

The correspondent process is modeled using Forge® 4.0 Finite Elements software from Transvalor. Axisymmetric conditions are supposed, for this, a 2D simulation with rigid dies is performed (see Fig. 4). Tetrahedral meshing elements were used. The length of a mesh edge averaged 0.6 mm in the core of the billet and was refined to 0.3 mm in the external parts. The finite elements ranged from 6000 to 12,000, depending on the billet's dimensions. Default FORGE® solver remeshing was activated during the simulations, and each run required an average of 15 min. The geometries, deformation fields, and load-height curves are extracted for further analysis. Material physical properties are listed in Table 1.

A reduced Hensel-Spittel law for copper rheology has been used to represent the billet's rheology. The flow stress σ_s is expressed as follows:

$$\sigma_s = A \cdot e^{m1 \cdot T} \cdot \epsilon^{m2} \cdot \dot{\epsilon}^{m3} \cdot e^{m4/\epsilon} \tag{1}$$

Here, ϵ and $\dot{\epsilon}$ are strain and strain rate respectively; T is the temperature; $A, m1, m2, m3, m4$ are material constants, with specific values of 411.19 MPa, -0.00121, 0.21554, 0.01472, and – 0.00935 respectively. These coefficients were taken from the Forge® material library database. Moreover, thermal exchanges have been assumed at $2000\ W/m^2\ K$ between the billet and the tools, and at $10\ W/m^2\ K$ between the air and the billet. Friction conditions are assumed from the literature [34, 35], following a Coulomb-limited Tresca Model [36]:

$$\tau = \min\left(\mu \cdot \sigma_n; \bar{m} \cdot K\right) \tag{2}$$

where σ_n is the contact pressure; K is the shear yield stress; μ and $\bar{m}$ are the Coulomb and Tresca friction coefficients, denoted by 0.1 and 0.2, respectively. This numerical model was validated against experimental data in our previous work [37] to ensure its accuracy. For four different experimental tests, the root mean squared error in geometry reconstruction of this numerical model for the geometries stands below 0.06 mm for the first blow. This ensures that the surrogate model database is grounded in a reliable numerical simulation.

Methodology

The methods employed to create a predictive model for forging operations are outlined in chronological order in Fig. 5. The initial step involves setting up a precise numerical simulation, which entails defining numerous parameters. This simulation is then subjected to model reduction techniques. In the presented use case, reduced-order modeling and parametrization techniques are employed. Through model reduction, a simplified representation of the operation is attained. This simplified model is subsequently used to train and validate a surrogate model. In this study, an artificial neural network multilayer perceptron is chosen as the training algorithm.

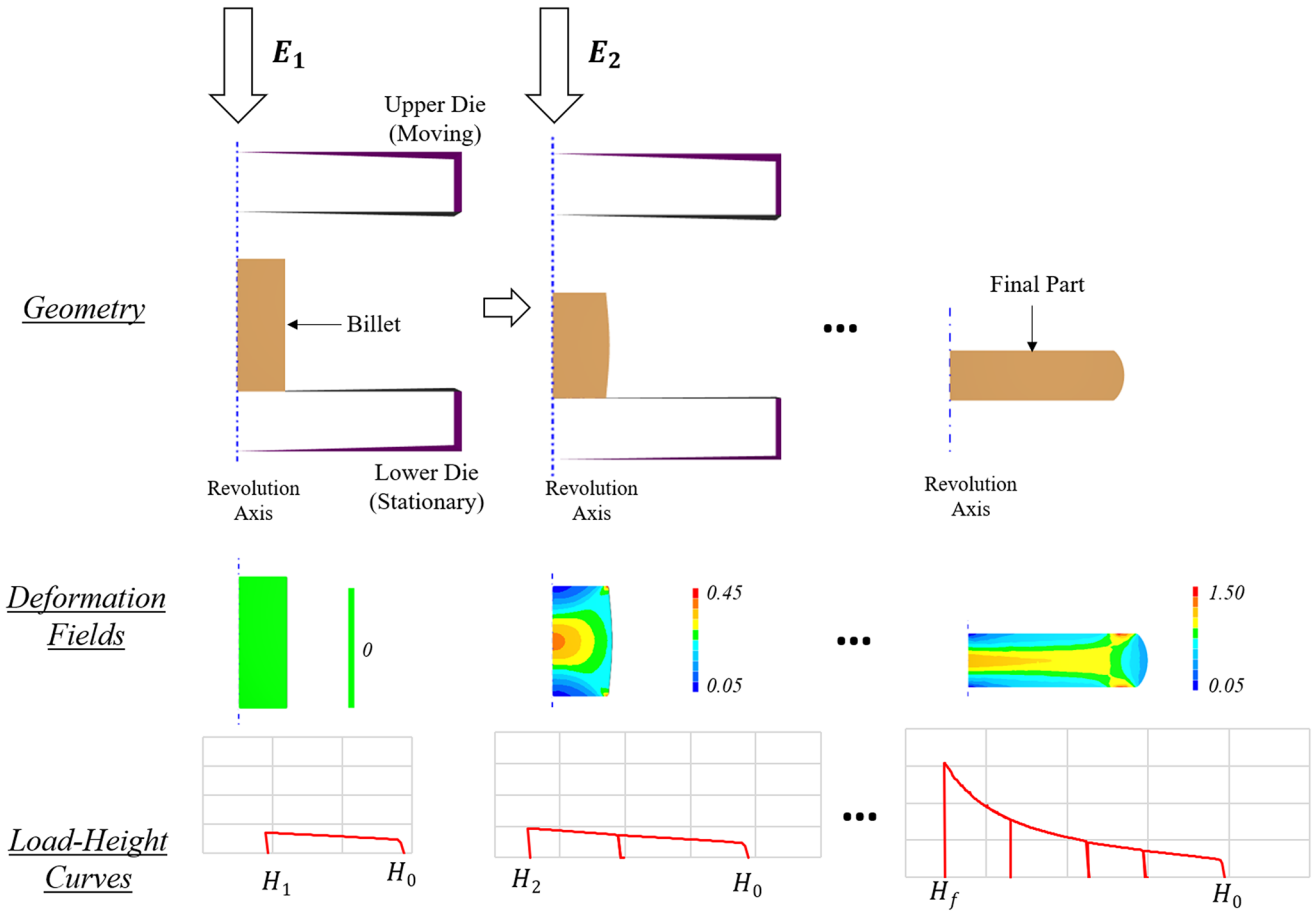

Fig. 4 Multiple-blow upsetting: numerical simulation

Table 1 Physical properties of billet at 20 °C

Material	Young's Modulus (MPa)	Poisson's ratio	Density (kg/m3)	Thermal Conductivity (W/m-K)	Specific Heat (J/kg-K)
Rolled Pure Copper	110,000	0.3	8100	401	435

The surrogate model, which reflects the billet's behavior, is subsequently coupled with a mass-spring-damper model to consider the dynamic interaction between the press, tooling, and billet. This dynamic behavior is not explicitly modeled within the numerical simulation framework. Detailed descriptions of each development step are provided in the subsequent sections.

Model reduction

The selected inputs and outputs for the surrogate model are illustrated in Fig. 6. Among these variables, the geometries of billets and deformation fields present specific challenges due to their susceptibility to the curse of dimensionality [38]. Billet geometries are commonly represented as scatter plots of 2D points or curves, typically comprising 30–80 data points. Conversely, deformation fields are represented as a scatter of 3D points (x, y, ϵ), with mesh-dependent size, ranging from 6000 to 12,000 points. In the pursuit of efficient surrogate model development, model reduction techniques are essential for managing high-dimensional data effectively.

In our previous work [26], we introduced a method to address geometry concerns associated with these features. To tackle the complexity of billet geometry, we employed a curve-parametrized representation with Bézier control points [39]. This approach facilitated dimensionality reduction by condensing the representation to only five control points, thereby resulting in a total of 10 data points (two spatial coordinates for each control point) (refer to Fig. 7a). Furthermore, under cold forging conditions, billets can be presumed to exhibit symmetry in their upper and lower parts [40]. Leveraging this symmetry enabled a more compact representation employing only five parameters, namely $x_1, x_2, x_3, y_2 \, and \, H$ (refer to Fig. 7b). Notably, the reconstruction errors using Bézier curves remained consistently

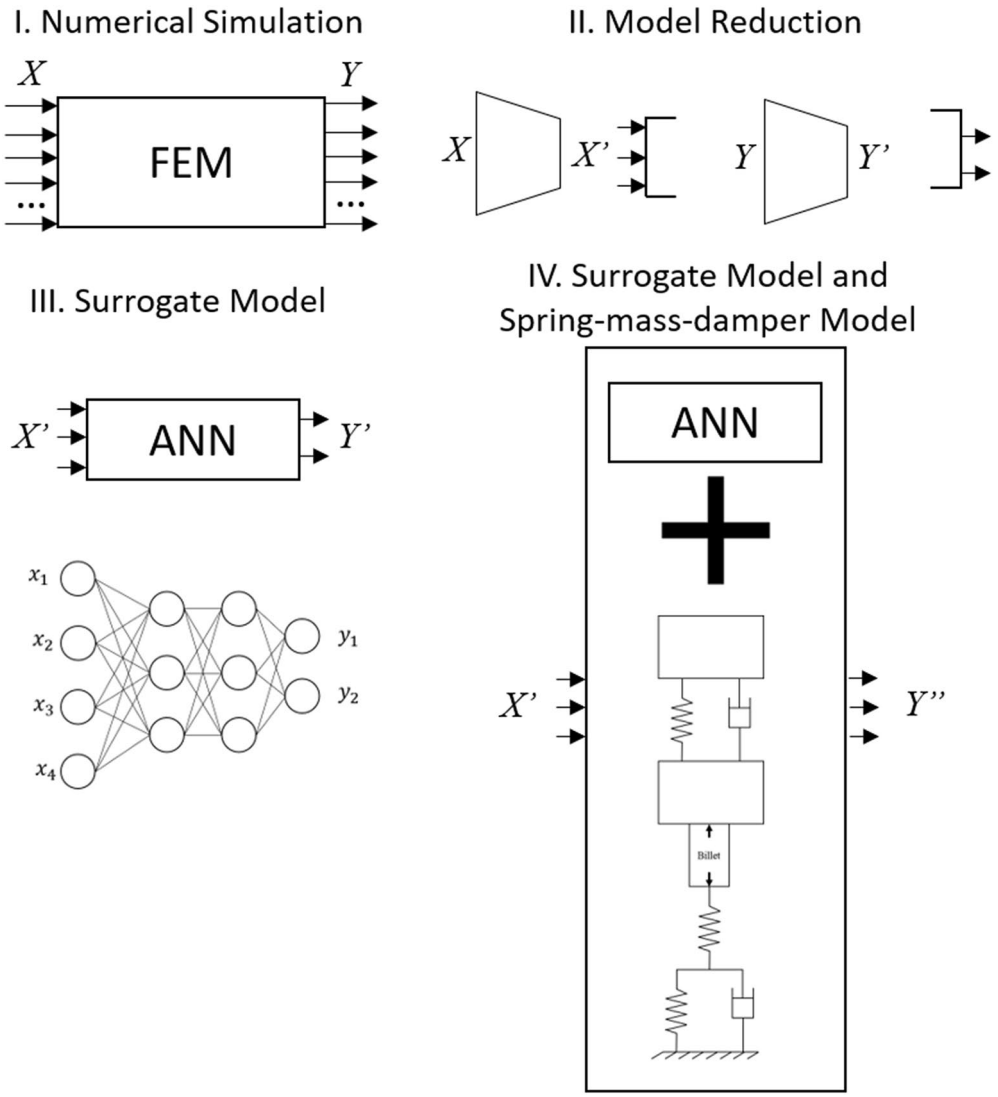

Fig. 5 Techniques Employed for Accurate Coupled Modeling in Forging Operations

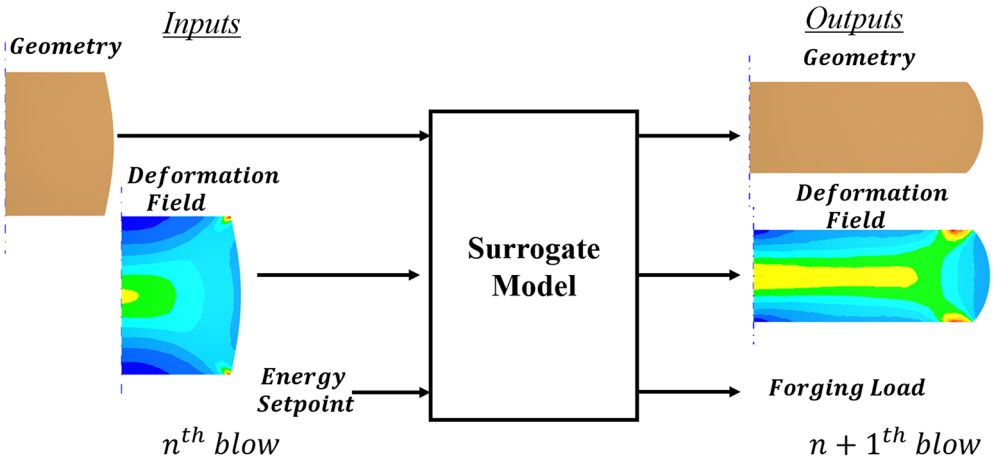

Fig. 6 Surrogate model's inputs and outputs

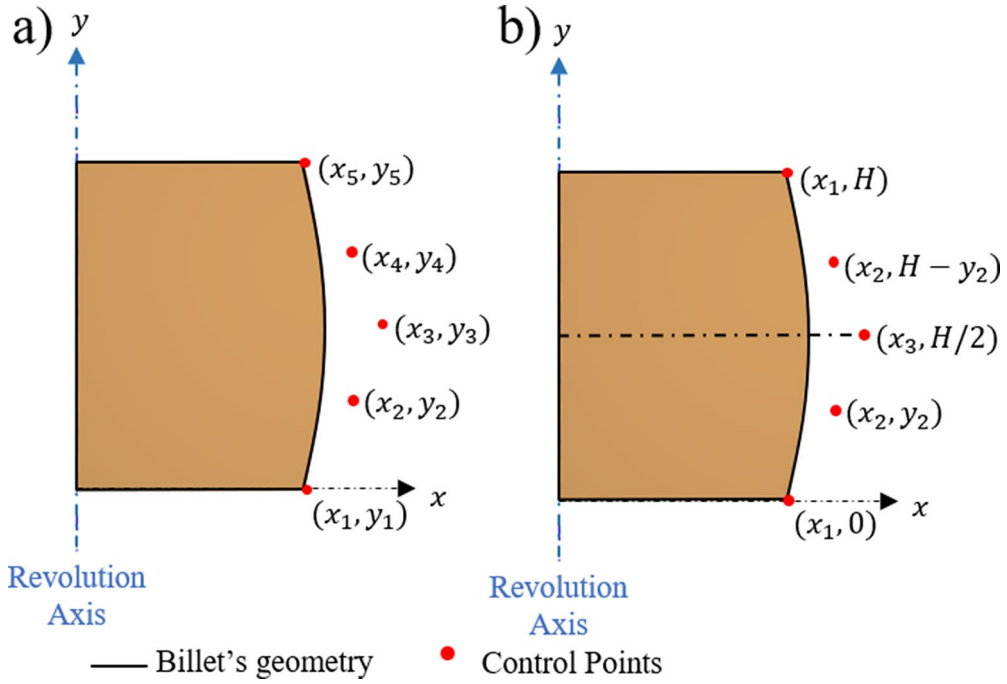

Fig. 7 Geometry parametrization using Bézier's Control Points

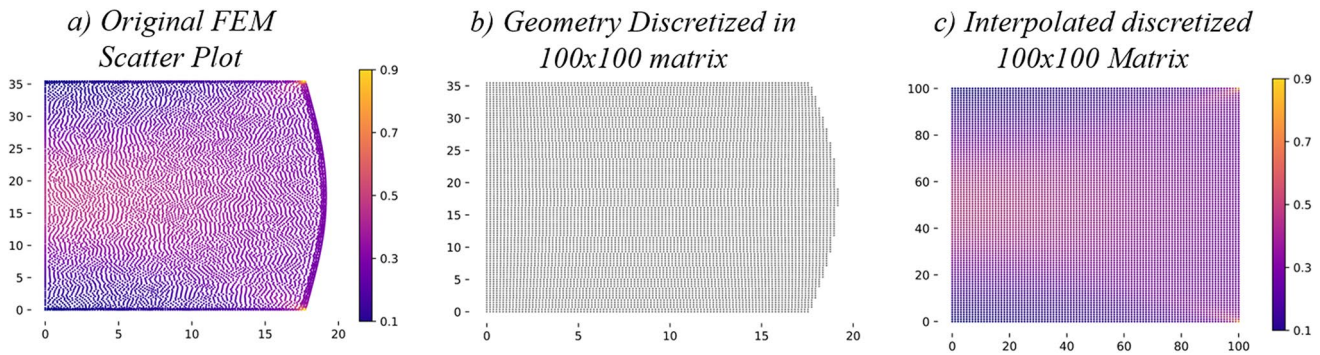

Fig. 8 Deformation field discretization: **a**) Original FEM. **b**) Geometry discretization. **c**) Deformation field discretization

below 0.026 mm for the root mean squared error, attesting the fidelity of the approach.

Regarding the deformation field, the original Finite Element Method (FEM) scatter plot was discretized based on the billet's geometry (Fig. 8). The deformation values were then interpolated using the Delaunay Triangulation method to generate consistent 100×100 matrices for each deformation field, as described in [26]. This discretization process is applied to each FEM deformation field, facilitating the construction of the snapshot matrices used in the Proper Orthogonal Decomposition (POD) reduction.

Subsequently, a reduction in basis eigenvectors was conducted utilizing the POD Method, which is based on Singular Value Decomposition [41]. The first three basis eigenvectors were retained, achieving a reconstruction mean absolute error of 0.0121 [mm/mm] and cumulative energy of 81.77% within deformation values reaching 1.5 [mm/mm]. This reduction enables the reconstruction of deformation fields using only three variable coefficients, which are subsequently multiplied by their corresponding basis vectors:

$$X = \sum {}_{i=1}^{3} b_i \cdot \varnothing_i \tag{3}$$

Where X is the reconstructed field; $\varnothing_i$ is the i_{th} basis eigenvector or mode obtained from the POD; and, b_i is the coefficient associated with the i_{th} mode.

Surrogate model

As the copper deformation is performed under cold forging conditions (where $T/T_{solidus} < 0.3$), atomic thermal agitation is minimal. This means that athermal mechanisms, which are less time-dependent and which are dominated by

processes such as dislocation movement, generally prevail [42]. Consequently, time-dependent metallurgical phenomena, such as recrystallization, diffusion, and restoration, are negligible at these cold temperatures. In this context, since these temporal phenomena are not considered, the surrogate model, with nine inputs and nine outputs retained after reduction, does not incorporate time factors.

To efficiently manage the high dimensionality of the model, a simulation-based database is constructed using the Design of Experiments (DoE) Latin Hypercube Sampling method, a widely employed technique in metal forming applications [43, 44]. A total of 2000 combinations were generated, each representing a numerical simulation. To achieve this, a Python script was executed using Forge® version 4.0's API interface. This script automated the data setup for simulations based on DoE combinations, which were stored in a .csv file. This operation facilitated the generation of the. tpf simulations file. The surrogate model architecture is constructed utilizing multilayer perceptron artificial neural networks (MLP-ANN) in Python, employing the Keras API, a framework commonly used in metal forming applications [45–47]. Three hidden layers consisting of 48, 192, and 48 neurons are retained, with ReLu activation functions applied, and a linear activation function is chosen for the output layer (refer to Fig. 9). The mean squared error (MSE) loss function is chosen, a common choice for training regression problems [48].

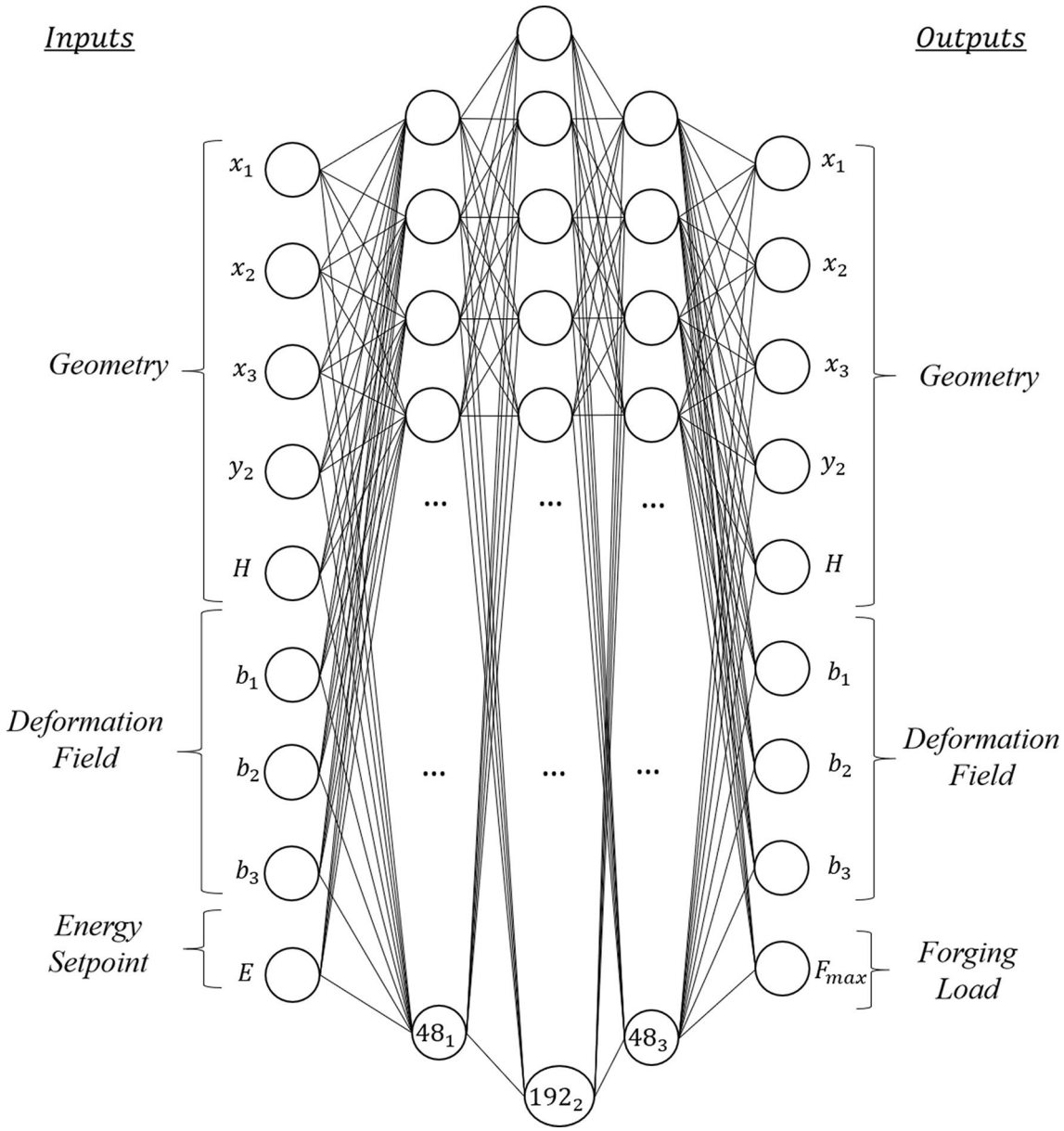

Fig. 9 ANN-MLP architecture

The simulation's database is normalized and divided into training, validation, and test data sets. The computation time is lower than 200ms. When the model is iteratively evaluated with a set of input variables, specifically by varying the energy from $E = [0, Energy_{max}]$, a series of points representing the load-displacement relationship can be obtained (see Fig. 10). Additionally, an energy-height curve can be extracted from the same evaluations.

Surrogate model and spring-mass-damper model coupling

The surrogate model facilitates the prediction of the geometry, deformation field, and forging load after the upsetting operation. However, its accuracy is compromised, as it assumes that all the energy contained in the Energy Setpoint input is transformed into deformation energy for forging the billet. In actual forging conditions, energy losses occur from the first blow onwards, and they increase with each subsequent blow as the operation progresses from soft to hard blows [37]. These energy losses can be accounted for by integrating the efficiency of each blow into the system:

$$\gamma = \frac{E_b}{E} = \frac{E - E_{losses}}{E} \tag{4}$$

Here, E_b is the deformation energy transferred to the billet, E denotes the energy setpoint or the available kinetic energy, and E_{losses} represents the cumulative energy losses, including friction, vibrations, and elastic deformation of the press and tooling. To determine the blow efficiency, one should model the billet, the machine-specific dynamic behavior, and their interactions, as done by [49], where a mass-spring-damper model (denoted BIM for Billet-Interface-Machine model) is specifically tailored for the same LASCO SPR400 screw press as this study (Fig. 11).

The BIM model tracks the initial kinetic energy, which decreases as the ram transfers this energy to the system, converting it into various other forms of energy. For the calculation, the BIM model needs access to the billet's forging load for a given displacement. The surrogate load-displacement curve obtained from the surrogate model is the input of the BIM model, which will give a real-time prediction of the blow's final heights ($H_1, H_2, \ldots, H_f$), the blow's efficiencies, the energy repartition and a corrected load-displacement curve (see Fig. 12).

Using this BIM model, the total energy could be deployed in five energies: the kinetic of the masses, the elastic energy stored within the springs, the dissipation of damping energy by the dampers, the frictional energy between the tools and the billet, and the plastic energy transferred to the billet. It should be noted that it is assumed that other losses, such as acoustic energy, are negligible compared to these five.

Coupling the BIM and the surrogate models should allow an accurate real-time prediction of the final height, the maximum load, and the blow efficiency for a multiple-blow operation. This approach could also be applied to other forming machines, as the model's coefficients can be calibrated for each different tooling and press configuration to achieve optimal predictions in different forging setups.

Results

To validate the predictive capability of the model for multiple blows, an experimental campaign was conducted. The model was trained using billets with initial diameters (D_0) ranging from 15 mm to 35 mm. Real billets with D_0 of 24.00 mm and 32.00 mm, along with various slenderness

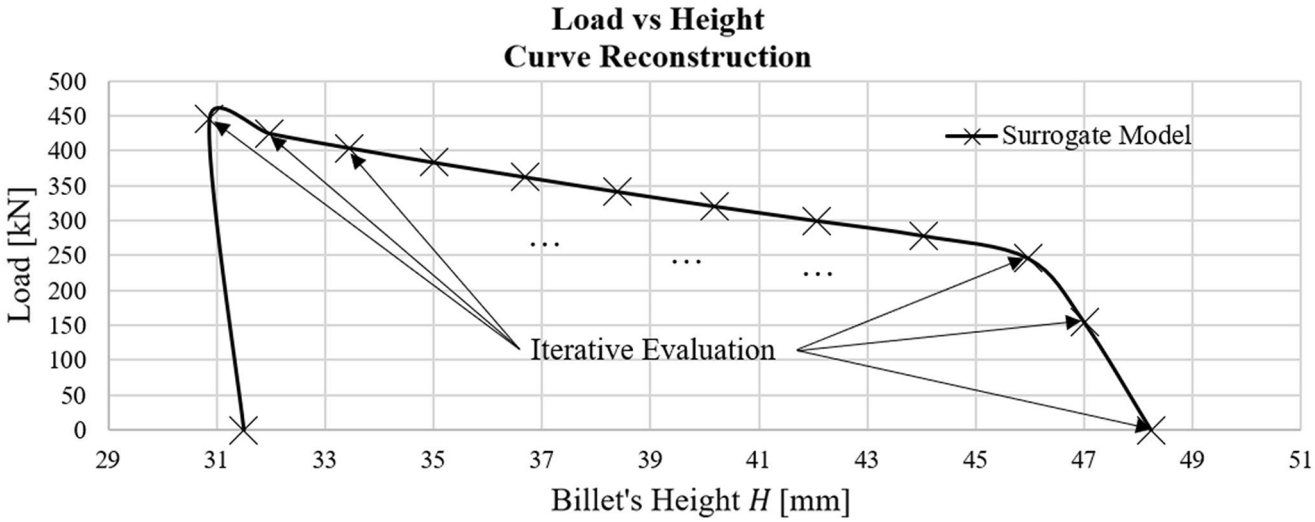

Fig. 10 Load-height curve obtained from an iterative evaluation of the surrogate model FH=[IF, FH]

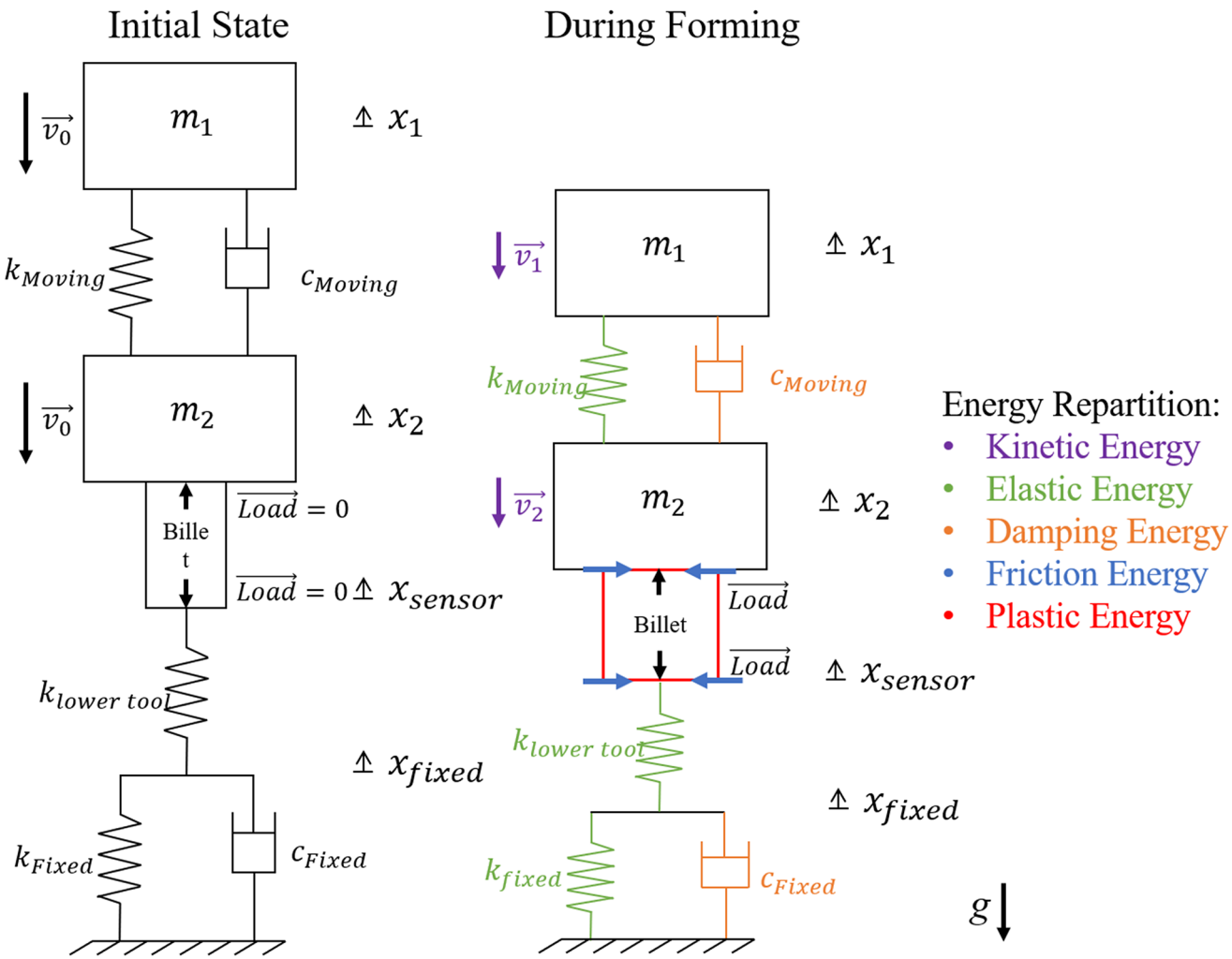

Fig. 11 Billet-Interface-Machine (BIM) model for the screw press (Initial State and During Forming). Edited from [49]

ratios not included in the training database, were forged as part of the validation process. Each billet underwent four forging cycles at different energy setpoints (Table 2). These energy levels were selected to ensure that the compression ratio remained below 80% in the fourth blow for all the billets.

The evolution of geometry is depicted for each of the four billets. Experimental, Finite Element Method (FEM), and Surrogate Model (SM) results are illustrated in Fig. 13 FEM-predicted billets exhibit greater deformation compared to SM-predicted ones after each blow. This discrepancy can be attributed to the inclusion of blow efficiency in the SM model. Despite potential cumulative errors in the SM predictions after 4 blows, they remain accurate relative to the FEM results. The mean absolute error between the experimental profiles and the SM ones stands at 0.1 mm, with a mean absolute percentage error below 1%.

It should be noted that the efficiency of each blow could be included in the FEM parameters. However, calculating the efficiency for each blow requires additional computation before integrating it into the simulation. In contrast, with the BIM approach, efficiency is automatically accounted for without the need for additional computations once the press-tooling model is identified.

To validate the deformation field, new FEM simulations were conducted under realistic conditions, incorporating accurately predicted plastic energy. This enabled a comparison between FEM and SM predictions. Figure 14a displays deformation field predictions and comparisons against FEM results for Billet 1 at the final blow, where more propagation of error is occurring. Figure 14b shows the difference between FEM and SM predictions for the same billet at the same blow. The figures display half of a 3D billet so the core deformation field can be seen.

For all the billets, the results indicate a mean absolute error below 0.05 [mm/mm] across a deformation field range of [0-1.5]. However, these errors are mainly concentrated in the corners of the billet and are primarily related to the

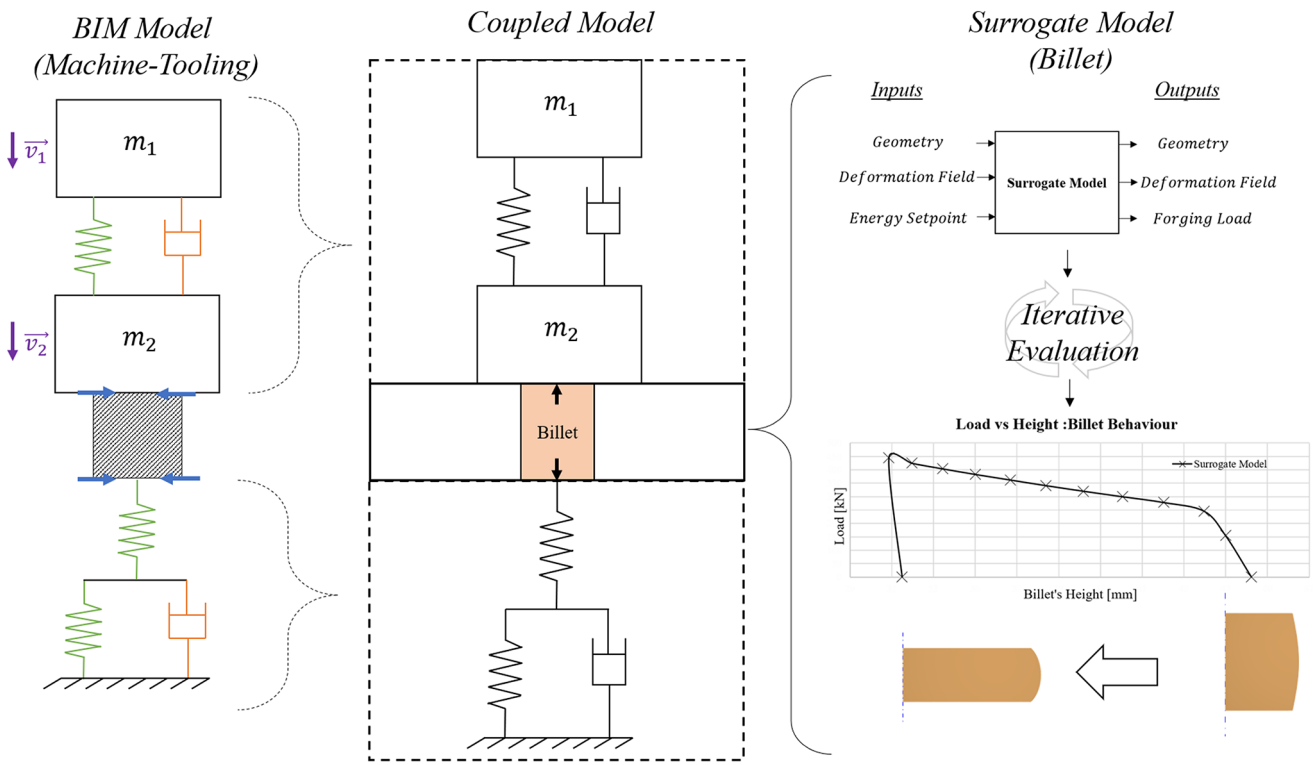

Fig. 12 Integration of the surrogate model in the BIM model. Coupling nature: weak (no continuous interaction between the two models)

Table 2 Experimental validation: summary

Billet	Initial Diameter [mm]	Initial Height [mm]	$Energy_1$[kJ]	$Energy_2$[kJ]	$Energy_3$[kJ]	$Energy_4$[kJ]
1	32.00	44.30	4.04	2.89	2.89	2.89
2	32.00	56.85	8.67	2.89	7.22	8.67
3	24.00	37.75	2.31	2.02	1.44	1.44
4	24.00	33.20	1.15	1.44	2.89	2.02

discretization of the field and the interpolation technique used to obtain these boundary values.

The load-displacement curves obtained from the coupled model closely matched the experimental data, with the prediction of billet heights showing an error below 5%, corresponding to 0.6 mm (refer to Fig. 15).

Furthermore, the prediction of blow efficiency was assessed, revealing maximum errors below 2.5% and a mean absolute error of 1.1% (see Fig. 16b). Across all billets, blow efficiency was found to decrease after each blow. Specifically, the initial blows are located in the upper right part of the Fig. 16a plot, while the subsequent blows are progressively positioned towards the lower left side.

A graphical representation of the energy distribution is presented in Fig. 17. It reveals that elastic energy consistently accounts for the majority of energy losses. Damping energy appears relatively low in the initial blows, remaining below 1% of the total losses. Frictional energy, on the other hand, shows an increase after the first blow followed by a decrease after the third blow. This observation can be attributed to the decrease in compression ratio of the billets after the third blow, as they become hardened. Consequently, less material flows between the billet and the tools. Friction energy, like damping energy, also remains below 1% of the losses for all the blows. It is important to mention that special attention should be paid to this analysis, as the values are presented as percentages of different energy setpoint values, and they are influenced by factors beyond just these energy setpoints, such as billet geometries and work-hardened states.

Discussion

The coupled model was evaluated in four-time blow upsetting operations and compared to experimental data on four different billets. The geometry predictions of the coupled model surpassed those of the FE model, displaying a MAE

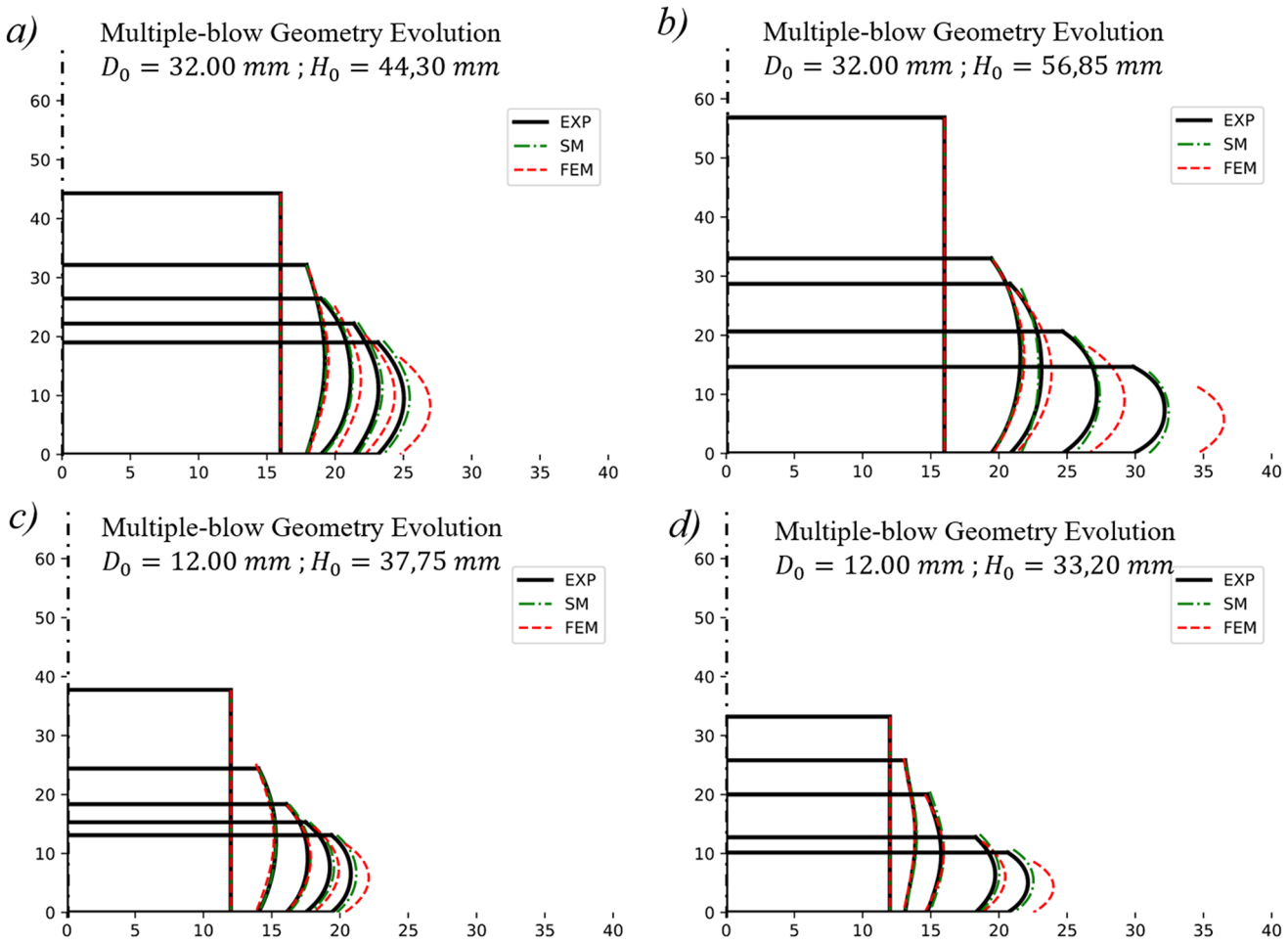

Fig. 13 Multiple-blow geometry evolution: a)$D_0 = 32.00\ mm\ ; H_0 = 44,30\ mm$. b)$D_0 = 32.00\ mm\ ; H_0 = 56,85\ mm$. c) $D_0 = 24.00\ mm\ ; H_0 = 37,75\ mm$. d) $D_0 = 24.00\ mm\ ; H_0 = 33,20\ mm$

below 0.1 mm and a MAPE below 1%. This underscores the importance of blow efficiency in multiple-blow operations, as evidenced by the decreasing accuracy of FE predictions with diminishing blow efficiency.

The use of the BIM model allows for the automatic distribution of energy among the various elements, eliminating the need to calculate efficiency for each blow separately, which would be required in FEM to achieve similar results.

The comparison between the deformation field SM prediction and the FEM one revealed errors below 0.05 mm/mm. The primary error location, typically found at the corners of the billets, was attributed to the discretization and interpolation of the fields, while their magnitude was linked to information loss during the model reduction process.

Apart from geometry and deformation field predictions, the model accurately estimated the load-displacement curves for multiple-blow operations, as well as the blows' efficiency and energy distribution. While the load-displacement curves prediction closely mirrored the actual process, exhibiting nearly overlapping curves (refer to Fig. 15), the accuracy decreased from less than 1% in the 1st blow to almost 5% in the 4th blow for the final height prediction. This limitation was attributed to factors such as initial prediction errors propagating with subsequent blows and nearing the training limits of the model due to a considerable increase in the billet compression ratio.

The blow's efficiency prediction closely aligned with experimental results, with a mean absolute error below 1.1%. The observed energy distribution aligned with findings from the literature on copper upsetting using a screw press [49]. Notably, elastic energy increased after each blow, while friction energy peaked in the first blow before declining with compression ratio and blow efficiency. Damping energy exhibited a slight increase but remained less significant compared to elastic and frictional energies.

Previously, blow efficiency calculations often relied on integrating data from numerical or analytical models post hoc into the BIM model. However, predictive surrogate modeling now enables efficiency calculations before forging begins. To enhance the model's accuracy and reliability,

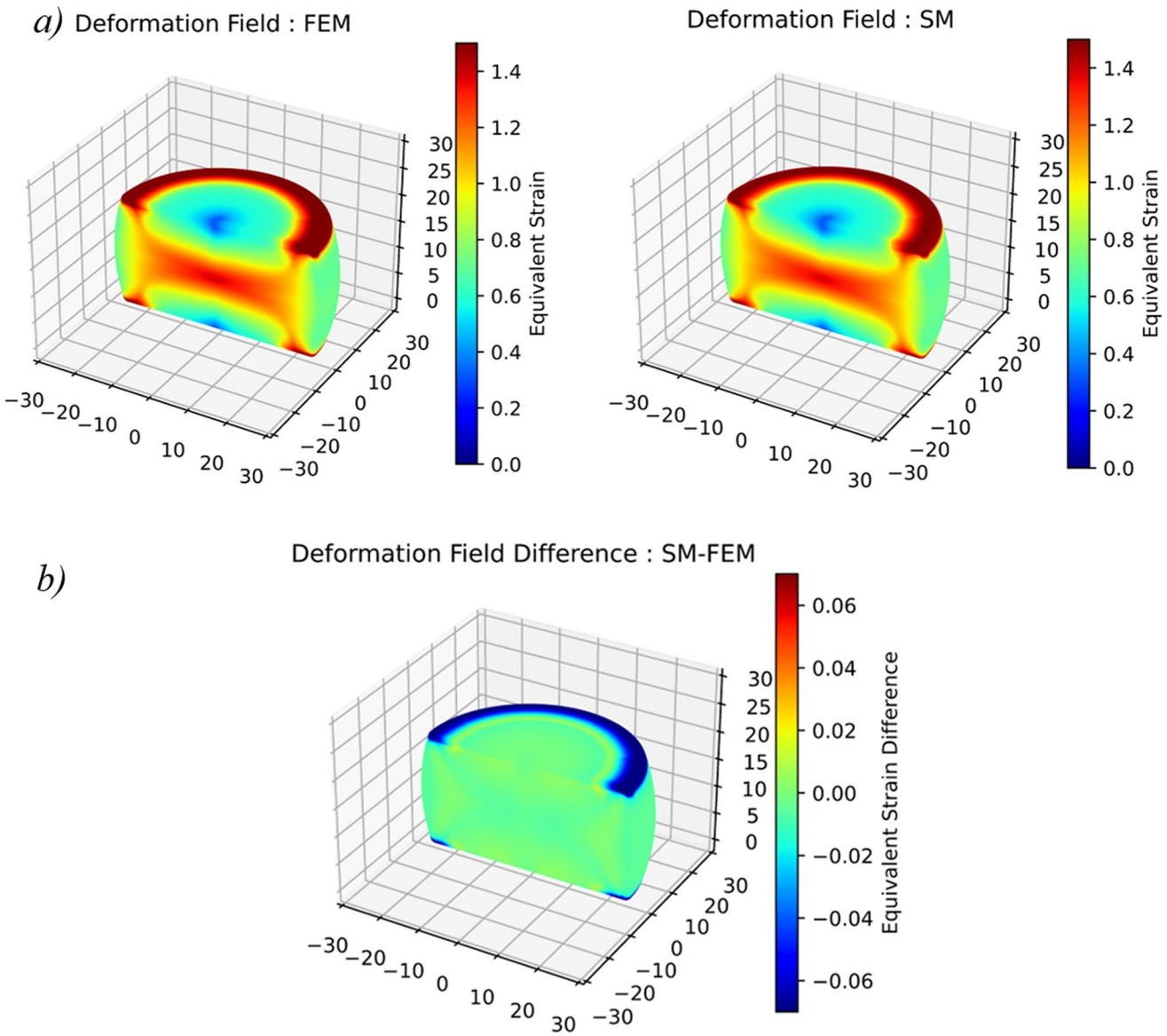

Fig. 14 Deformation field results for Billet 1 $(\boldsymbol{D}_0 = 32.00\,\boldsymbol{mm}\,;\boldsymbol{H}_0 = 44,30\,\boldsymbol{mm})$ at the 4th blow: **a)** FEM and SM results. **b)** Difference between SM and FEM [SM-FEM]

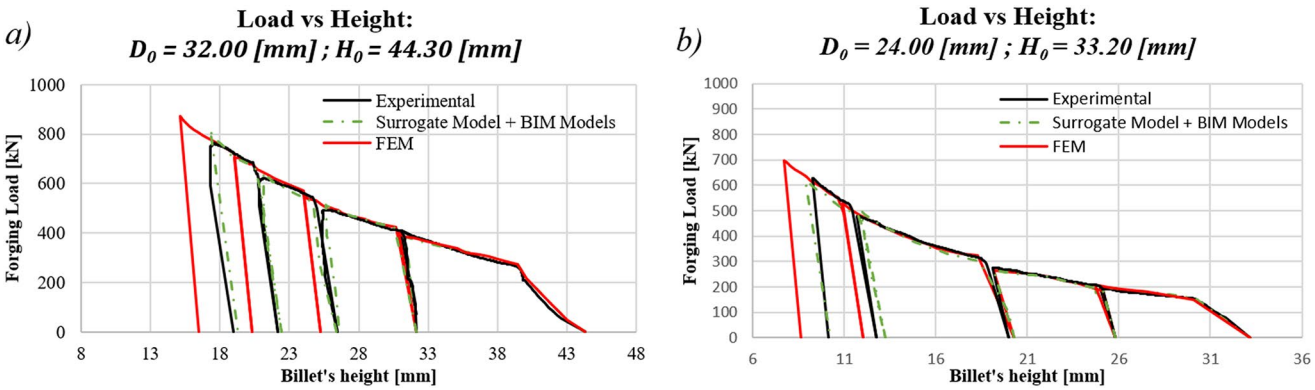

Fig. 15 Load-displacement curves: experimental and coupled model. **a)** $\boldsymbol{D}_0 = 32.00\,\boldsymbol{mm}\,;\boldsymbol{H}_0 = 44,30\,\boldsymbol{mm}$. **b)** $\boldsymbol{D}_0 = 24.00\,\boldsymbol{mm}\,;\boldsymbol{H}_0 = 33,20\,\boldsymbol{m}$

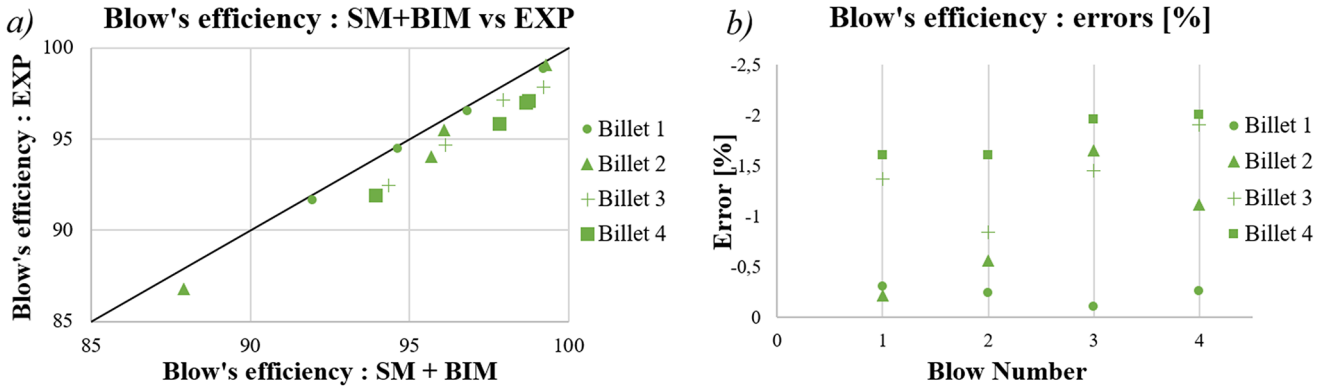

Fig. 16 Blow's efficiency results

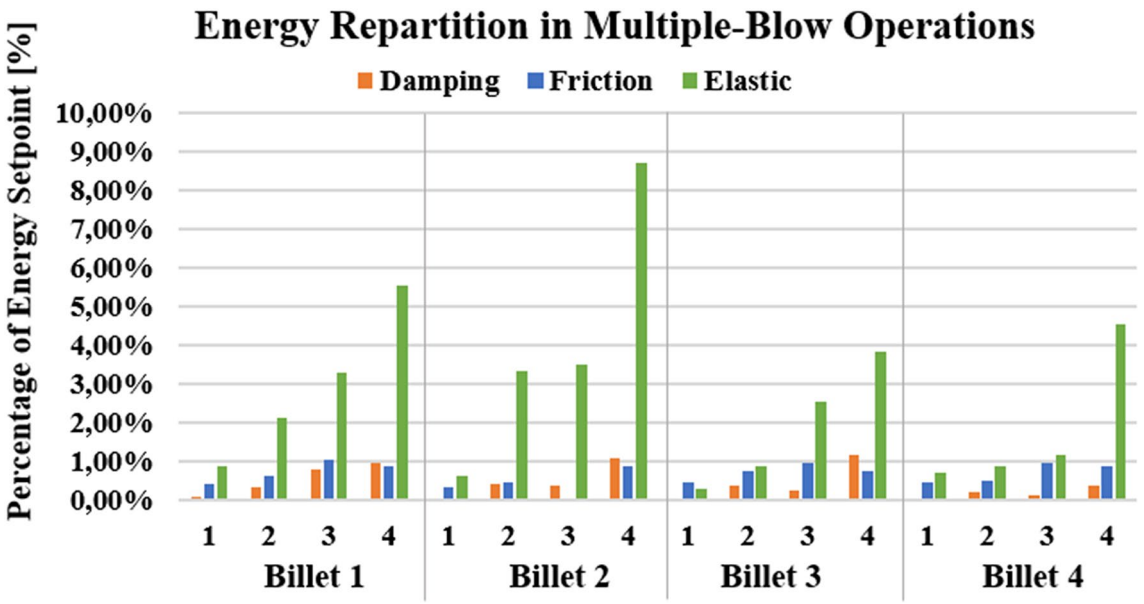

Fig. 17 Energy Repartition from SM + BIM Model for multiple-blow upsetting

additional process variables such as billet temperature, press ram velocity, or friction conditions should be incorporated. Additionally, exploring adjustment techniques based on actual process outcomes after each blow is crucial to minimize error propagation by the fourth blow.

The coupled model demonstrated high accuracy in predicting geometry, deformation fields, and load-displacement curves, underscoring its effectiveness in axisymmetric multiple-blow upsetting operations. Extending this methodology to more complex forging scenarios, such as those involving anisotropic materials or full 3D models, would require careful consideration of numerical model validation, model reduction algorithms, dataset size, and surrogate model training and validation. While the general approach remains applicable, adapting the tools and methods to accommodate these complexities is crucial.

Conclusions and perspectives

The proposed methodology integrates a billet-related surrogate model into a Billet-Interface-Machine (BIM) interactions model. The surrogate model enables the prediction of the billet's geometry, deformation field, and load-height behavior for multiple-blow upsetting operations. The geometry of the billets is parameterized using Bézier curves, resulting in five geometric parameters. The deformation fields are reduced using a Proper Orthogonal Decomposition (POD) framework, leading to three parameters for describing them. The database for the surrogate model is obtained from numerical simulations. The surrogate model employs a multilayer perceptron artificial neural network with three hidden layers. The load-height behavior predicted by the surrogate model serves as input for the BIM model, which simulates the billet's interaction with the forging machine over multiple blows. This model allows the prediction of

blow efficiency and energy distribution (plastic, elastic, damped, and frictional energies), going beyond numerical simulation predictions, resulting in accurate results.

In future work, continuous refinement of the coupled model after each blow will be essential to minimize error propagation. This iterative refinement process may lead to the development of a so-called hybrid model, which considers the inherent uncertainties present in each individual model, ensuring the model's accuracy and reliability.

Acknowledgements We extend our sincere thanks to CETIM for their financial support in this research project. We deeply appreciate the guidance of Valérie Sulis and Stéphane Magron in overseeing the project. A special acknowledgment to Francisco Chinesta, university professor and researcher at the Laboratory for Processes and Engineering in Mechanics and Materials (PIMM), for his invaluable advice. Lastly, we would like to express our gratitude to Sébastien Burgun and Daniel Boehm for their technical support during the tests.

Author contributions DU: Formal Analysis, Data curation, Software, Writing-original draft, Writing-review & editing; CD: Conceptualization, Validation, Writing-review & editing; CB: Methodology, Investigation, Writing-review & editing; RB: Resources, Supervision, Writing–review & editing, Funding acquisition.

Funding This study was funded by the Technical Center for Mechanical Industry (CETIM) and the Carnot Institut ARTS (Research Actions for Technology and Society).
Open access funding provided by Arts et Metiers Institute of Technology.

Declarations

Competing interests The authors have no competing interests to declare that are relevant to the content of this article.

References

1. Jasleen Kaur BS, Pabla SS, Dhami, Chandigarh NITTTR (2016) A Review on Field Areas of Research in Forging Process using FEA, *Int. J. Eng. Res.*, vol. V5, no. 01, p. IJERTV5IS010310, Jan. https://doi.org/10.17577/IJERTV5IS010310
2. Vajpayee S, Sadek MM (May 1978) Effects of Structural and forming parameters on the Efficiency of Energy Transfer in Impact Forming machines. J Eng Ind 100(2):113–118. https://doi.org/10.1115/1.3439397
3. Vajpayee S, Sadek MM, Tobias SA (Jan. 1979) The efficiency and clash load of impact forming machines to the second order of approximation. Int J Mach Tool Des Res 19(4):237–252. https://doi.org/10.1016/0020-7357(79)90013-1
4. Durand C, Bigot R, Baudouin C (Jan. 2018) Contribution to characterization of metal forming machines: application to screw presses. Procedia Manuf 15:1024–1032. https://doi.org/10.1016/j.promfg.2018.07.391
5. Brecher C, Esser M, Witt S (Jan. 2009) Interaction of manufacturing process and machine tool. CIRP Ann 58(2):588–607. https://doi.org/10.1016/j.cirp.2009.09.005
6. Giorleo L, Ceretti E, Giardini C (2013) Energy consumption reduction in Ring Rolling processes: A FEM analysis, *Int. J. Mech. Sci.*, vol. 74, pp. 55–64, Sep. https://doi.org/10.1016/j.ijmecsci.2013.04.008
7. Tehel R, Päßler T, Bergmann M (Feb. 2020) Effective FE models for simulating the elasto-mechanical characteristics of forming machines. Int J Adv Manuf Technol 106:3505–3514. https://doi.org/10.1007/s00170-019-04832-6
8. Zheng E, Zhou X (Apr. 2014) Modeling and simulation of flexible slider-crank mechanism with clearance for a closed high speed press system. Mech Mach Theory 74:10–30. https://doi.org/10.1016/j.mechmachtheory.2013.11.015
9. Brecher C, Klein W, Tannert M (May 2010) Optimization of multi-stage closed-die forging processes by coupled simulation of the machine and the forging processes. Prod Eng 4(2):279–286. https://doi.org/10.1007/s11740-010-0226-5
10. Swidergal K et al (2015) Dec., Experimental and numerical investigation of blankholder's vibration in a forming tool: a coupled MBS-FEM approach, *Prod. Eng.*, vol. 9, no. 5, pp. 623–634, https://doi.org/10.1007/s11740-015-0640-9
11. Rojek J, Oñate E, Postek E (Aug. 1998) Application of explicit FE codes to simulation of sheet and bulk metal forming processes. J Mater Process Technol 80–81. https://doi.org/10.1016/S0924-0136(98)00169-1
12. Yang DY, Yoo YH (Jan. 1997) Analysis and design of Multiblow Hammer forging processes by the explicit dynamic finite element Method. CIRP Ann 46(1):191–194. https://doi.org/10.1016/S0007-8506(07)60806-3
13. Harwood M, Novak M (Apr. 1986) Uplift in hammer foundations. Soil Dyn Earthq Eng 5(2):102–117. https://doi.org/10.1016/0267-7261(86)90004-7
14. Novak M (1983) Foundations for shock-producing machines, *Can. Geotech. J.*, Accessed: Mar. 03, 2023. [Online]. Available: https://www.semanticscholar.org/paper/Foundations-for-shock-producing-machines-Novak/f97002aeeee038c94b7a122cba28b0addd79c4f0
15. Yang DY, Jung DW, Song IS, Yoo DJ, Lee JH (1995) Comparative investigation into implicit, explicit, and iterative implicit/explicit schemes for the simulation of sheet-metal forming processes, *J. Mater. Process. Technol.*, vol. 50, no. 1, pp. 39–53, Mar. https://doi.org/10.1016/0924-0136(94)01368-B
16. Benner P, Grivet-Talocia S, Quarteroni A, Rozza G, Schilders W, Silveira LM (eds) (2021) System- and data-driven methods and algorithms, vol 1. De Gruyter. https://doi.org/10.1515/9783110498967
17. Hürkamp A et al (2020) Combining Simulation and Machine Learning as Digital Twin for the Manufacturing of Overmolded Thermoplastic composites. J Manuf Mater Process 4(3):92. https://doi.org/10.3390/jmmp4030092
18. Gustafsson E (2007) Optimization of Castings by using Surrogate Models, Accessed: Jan. 04, 2022. [Online]. Available: http://urn.kb.se/resolve?urn=urn:nbn:se:liu:diva-10192
19. Ryser M, Bambach M (2021) Comparison of Linear Regression and Neural Networks as Surrogates for Sensor Modeling on a

Deep Drawn Part, in *Forming the Future*, Cham, pp. 611–623. https://doi.org/10.1007/978-3-030-75381-8_50
20. Cai L, Ren L, Wang Y, Xie W, Zhu G, Gao H Surrogate models based on machine learning methods for parameter estimation of left ventricular myocardium. R Soc Open Sci, 8, 1, p. 201121, https://doi.org/10.1098/rsos.201121
21. Slimani K, Zaaf M, Balan T (Mar. 2023) Accurate surrogate models for the flat rolling process. Int J Mater Form 16. https://doi.org/10.1007/s12289-023-01744-5
22. Hamdaoui M, Le Quilliec G, Breitkopf P, Villon P (2014) POD surrogates for real-time multi-parametric sheet metal forming problems, *Int. J. Mater. Form.*, vol. 7, no. 3, pp. 337–358, Sep. https://doi.org/10.1007/s12289-013-1132-0
23. Dang VT, Labergere C, Lafon P (Jan. 2017) POD surrogate models using adaptive sampling space parameters for springback optimization in sheet metal forming. Procedia Eng 207:1588–1593. https://doi.org/10.1016/j.proeng.2017.10.1053
24. Dang V-T, Labergère C, Lafon P (2019) Adaptive metamodel-assisted shape optimization for springback in metal forming processes, *Int. J. Mater. Form.*, vol. 12, no. 4, pp. 535–552, Jul. https://doi.org/10.1007/s12289-018-1433-4
25. Ryser M, Neuhauser FM, Hein C, Hora P, Bambach M (2021) Surrogate model–based inverse parameter estimation in deep drawing using automatic knowledge acquisition, *Int. J. Adv. Manuf. Technol.*, vol. 117, no. 3–4, pp. 997–1013, Nov. https://doi.org/10.1007/s00170-021-07642-x
26. Uribe D, Baudouin C, Durand C, Bigot R (Dec. 2023) Predictive control for a single-blow cold upsetting using surrogate modeling for a digital twin. Int J Mater Form 17(1):7. https://doi.org/10.1007/s12289-023-01803-x
27. Scandola L et al (2021) Sep., Development of a numerical compensation framework for geometrical deviations in bulk metal forming exploiting a surrogate model and computed compatible stresses, *Int. J. Mater. Form.*, vol. 14, no. 5, pp. 901–916, https://doi.org/10.1007/s12289-020-01603-7
28. Bambach M, Imran M, Sizova I, Buhl J, Gerster S, Herty M (May 2021) A soft sensor for property control in multi-stage hot forming based on a level set formulation of grain size evolution and machine learning. Adv Ind Manuf Eng 2:100041. https://doi.org/10.1016/j.aime.2021.100041
29. Cueto E, Chinesta F, Huerta A (2014) Model Order reduction based on proper orthogonal decomposition. In: Chinesta F, Ladevèze P (eds) in Separated representations and PGD-Based model reduction: fundamentals and Applications. Springer, Vienna, pp 1–26. https://doi.org/10.1007/978-3-7091-1794-1_1.
30. Chinesta F, Ladeveze P, Cueto E (2011) A Short Review on Model Order Reduction Based on Proper Generalized Decomposition, *Arch. Comput. Methods Eng.*, vol. 18, no. 4, pp. 395–404, Nov. https://doi.org/10.1007/s11831-011-9064-7
31. Midaoui A, Baudouin C, Florence D, Régis B (2024) Surrogate model to describe temperature field in real-time for hot forging. https://doi.org/10.21741/9781644903131-95
32. Uribe D, Baudouin C, Locard Y, Durand C, Bigot R (May 2024) Enhancing metal-forming predictions with VR-infused digital twin models. 2309–2319. https://doi.org/10.21741/9781644903131-254
33. de Gooijer B, Havinga J, Geijselaers H, Van den Boogaard T (Dec. 2021) Evaluation of POD based surrogate models of fields resulting from nonlinear FEM simulations. Adv Model Simul Eng Sci 8. https://doi.org/10.1186/s40323-021-00210-8
34. Altan T, Ngaile G, Shen G (eds) (2004) Cold and hot forging: fundamentals and applications. ASM International, Materials Park, OH
35. Belur BK, Grandhi RV (Oct. 2004) Geometric deviations in forging and cooling operations due to process uncertainties. J Mater Process Technol 152(2):204–214. https://doi.org/10.1016/j.jmatprotec.2004.02.064
36. Zhang D-W, Xu F-F, Yu Z-C, Lu K-Y, Zheng Z-B, Zhao S-D (Jun. 2021) Coulomb, Tresca and Coulomb-Tresca friction models used in analytical analysis for rolling process of external spline. J Mater Process Technol 292:117059. https://doi.org/10.1016/j.jmatprotec.2021.117059
37. Uribe D, Durand C, Baudouin C, Krumpipe P, Bigot R (2023) Towards the Real-Time Piloting of a Forging Process: Development of a Surrogate Model for a Multiple Blow Operation, in *Proceedings of the 14th International Conference on the Technology of Plasticity - Current Trends in the Technology of Plasticity*, Cham, pp. 377–388. https://doi.org/10.1007/978-3-031-41341-4_39
38. Raisee M, Kumar D, Lacor C (2015) A non-intrusive model reduction approach for polynomial chaos expansion using proper orthogonal decomposition. Int J Numer Methods Eng 103(4):293–312. https://doi.org/10.1002/nme.4900
39. Fitter HN, Pandey AB, Patel DD, Mistry JM (Jan. 2014) A review on approaches for handling Bezier curves in CAD for Manufacturing. Procedia Eng 97:1155–1166. https://doi.org/10.1016/j.proeng.2014.12.394
40. Fan J, Liu Z, Liu W, Wang C (Jan. 2023) Simulation and Experiment Study on Cone End Billet Method in Upsetting Billet with a large height-to-diameter ratio. Appl Sci 13 17, Art. 17. https://doi.org/10.3390/app13179523
41. Schilders W (2008) Introduction to Model Order reduction. In: Schilders WHA, van der Vorst HA, Rommes J (eds) Model Order reduction: theory, Research Aspects and Applications. Springer, Berlin, Heidelberg, pp 3–32. doi: https://doi.org/10.1007/978-3-540-78841-6_1.
42. Montheillet F (2008) Métallurgie en mise en forme à froid, Mise en forme des métaux et fonderie. Editions Techniques de l'Ingenieur, Dec. 2008, https://doi.org/10.51257/a-v1-m3030.
43. Fays S, Baudouin C, Langlois L, Borsenberger M, Balan T, Bigot R (May 2024) Compensation of billet variabilities through metamodel-based optimization in open die forging. Int J Adv Manuf Technol 132(3):1665–1678. https://doi.org/10.1007/s00170-024-13392-3
44. Zhu F, Wang Z, Lv M (Apr. 2016) Multi-objective optimization method of precision forging process parameters to control the forming quality. Int J Adv Manuf Technol 83(9):1763–1771. https://doi.org/10.1007/s00170-015-7682-1
45. Shang H, Wu P, Lou Y (2021) Strain Hardening of AA5182-O Considering Strain Rate and Temperature Effect, in *Forming the Future*, Cham, pp. 657–665. https://doi.org/10.1007/978-3-030-75381-8_54
46. Hedicke-Claus Y, Kriwall M, Langner J, Stonis M, Behrens B-A (2021) Validation of Automatically Generated Forging Sequences by Using FE Simulations, in *Forming the Future*, Cham, pp. 2867–2881. https://doi.org/10.1007/978-3-030-75381-8_238
47. Li S, Guo Z, Cheng S, Zhang X (Jan. 2014) Design optimization of sheet metal stamped parts by CAE Simulation and back-propagation neural network. Procedia Eng 81:1023–1028. https://doi.org/10.1016/j.proeng.2014.10.135
48. Brownlee J (2019) How to Choose Loss Functions When Training Deep Learning Neural Networks, *MachineLearningMastery.com*, Jan. 29, https://machinelearningmastery.com/how-to-choose-loss-functions-when-training-deep-learning-neural-networks/ (accessed Jan. 23, 2023)
49. Song H, Durand C, Baudouin C, Bigot R (2024) Dynamic modelling and efficiency prediction for forging operations under a screw press, *Int. J. Adv. Manuf. Technol.*, vol. 134, no. 1, pp. 645–656, Sep. https://doi.org/10.1007/s00170-024-14145-y